A Cohesive Zone Modeling Study on the Fracturing Behavior of Thermoset Polymer Nanocomposites

Yao Qiao
Marco Salviato
Paper Number: 19

July 1, 2018

ABSTRACT

This work proposes an investigation on the fracturing behavior of polymer nanocomposites. Towards this end, the study leverages the analysis of a large bulk of fracture tests from the literature with the goal of critically investigating the effects of the nonlinear Fracture Process Zone (FPZ).

It is shown that for most of the fracture tests, the effects of the nonlinear FPZ are not negligible, leading to significant deviations from Linear Elastic Fracture Mechanics (LEFM). By means of Size Effect Law (SEL) on the assumption of a linear cohesive crack law, the fracture tests in the literature were re-analyzed. As the data indicate, this aspect needs to be taken into serious consideration since the use of LEFM to estimate mode I fracture energy, which is common practice in the literature, can lead to an error as high as 157% depending on the specimen size and nanofiller content.

This was further confirmed by matching the data by means of a cohesive zone modeling featuring a linear cohesive law. Taking advantage of size effect tests on thermoset-based graphene nanocomposites, it was also found that these materials are better described by a bilinear cohesive law. It was shown that, while the use of a linear cohesive law provides a good approximation, a bilinear cohesive law provides a superior description of the fracturing behavior for different sizes.

Yao Qiao, Department of Aeronautics and Astronautics, University of Washington, Guggenheim Hall, Seattle, WA, 98195
Marco Salviato, Department of Aeronautics and Astronautics, University of Washington, Guggenheim Hall, Seattle, WA, 98195

INTRODUCTION

The outstanding advances in polymer nanocomposites have paved the way for their broad use in engineering. Potential applications of these materials include microelectronics [1], energy storage [2] and harvesting [3], soft robotics [4], and bioengineering [5]. One of the reasons of this success is that, along with remarkable enhancements of physical properties such as e.g. electric and thermal conductivity [6,7], nanomodification offers significant improvements of stiffness [8], strength [9] and toughness [10–12]. These aspects make it an excellent technology to enhance the mechanical behavior of polymers [13–26] or to improve the weak matrix-dominated properties of fiber composites [27, 28].

While a large bulk of data on the mechanical properties of polymer nanocomposites is available already, an aspect often overlooked is the effect on the fracturing behavior of the region close to the crack tip featuring most of energy dissipation, the *Fracture Process Zone* (FPZ). This is an important aspect since, due to the complex mesostructure characterizing nanocomposites, the size of the non-linear FPZ occurring in the presence of a large stress-free crack is usually not negligible [29–33]. The stress field along the FPZ is nonuniform and decreases with crack opening, due to a number of damage mechanisms such as e.g. discontinuous cracking, micro-crack deflection, plastic yielding of nanovoids, shear banding and micro-crack pinning [10–12, 20, 35–40]. As a consequence, the fracturing behavior and, most importantly, the energetic size effect associated with the given structural geometry, cannot be described by means of classical Linear Elastic Fracture Mechanics (LEFM) which assumes the effects of the FPZ to be negligible. To seize the effects of a finite, non-negligible FPZ, the introduction of a characteristic (finite) length scale related to the fracture energy and the strength of the material is necessary [29–33].

This work proposes an investigation on the fracturing behavior of thermoset polymer nanocomposites with the goal of critically investigating the effects of the nonlinear Fracture Process Zone (FPZ). By employing Size Effect Law (SEL), a formulation endowed with a characteristic length inherently related to the FPZ size, and assuming a linear cohesive behavior [34], a large bulk of literature data is analyzed. It is shown that for most of the fracture tests, the nonlinear behavior of the FPZ is not negligible, leading to significant deviations from LEFM. As the data indicate, this aspect needs to be taken into serious consideration since the use of LEFM to estimate mode I fracture energy can lead to an error as high as 157% depending on the specimen size and nanofiller content.

A linear cohesive crack modeling (LCM) was studied to further understand the fracturing behavior of polymer nanocomposites. It was shown that while the LCM with corrected fracture energy by SEL is capable of capturing experimental data, this is not the case for the LCM with the fracture energy calculated by LEFM, with the non-negligible unerestimation on the peak load of nanocomposites. This is the confirmation that Size Effect Law (SEL) can be adapted to re-analyze the fracture tests available in the literature for the first approximation. Taking advantage of size effect tests on thermoset-based graphene nanocomposites by Mefford *et al.* [12], it was also found that these materials are better described by a bilinear cohesive law. It was shown that, while the use of a linear cohesive law provides a good approximation,

a bilinear cohesive law provides a superior description of the fracturing behavior for different sizes.

QUASI-BRITTLE FRACTURE OF NANOCOMPOSITES

Size effect law for nanocomposites

The fracture process in nanocomposites can be analyzed leveraging an equivalent linear elastic fracture mechanics approach to account for the presence of a FPZ of finite size as shown in Figure 1. To this end, an effective crack length $a = a_0 + c_f$ with $a_0 =$ initial crack length and $c_f =$ effective FPZ length is considered. Following LEFM, the energy release rate can be written as follows:

$$G(\alpha) = \frac{\sigma_N^2 D}{E^*} g(\alpha) \tag{1}$$

where $\alpha = a/D =$ normalized effective crack length, $E^* = E$ for plane stress and $E^* = E/(1-\nu^2)$ for plane strain, $g(\alpha) =$ dimensionless energy release rate and, D is represented in Figure 2 for Single Edge Notch Bending (SENB) and Compact Tension (CT) specimens respectively. σ_N represents the nominal stress defined as e.g. $\sigma_N = 3PL/2tD^2$ for SENB specimens or $\sigma_N = P/tD$ for CT specimens where, following Figure 2, P is the applied load, t is the thickness and L is the span between the two supports for a SENB specimen as defined in ASTM D5045-99 [41].

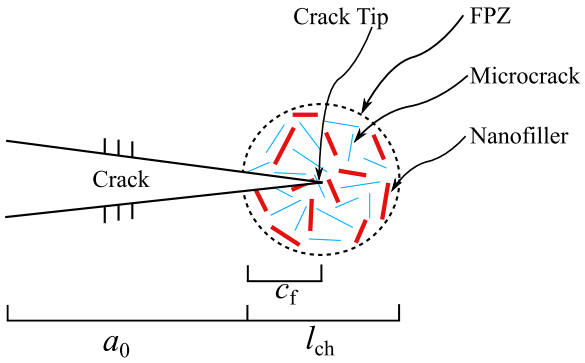

Figure 1. Fracture Process Zone (FPZ) for thermoset polymer nanocomposites.

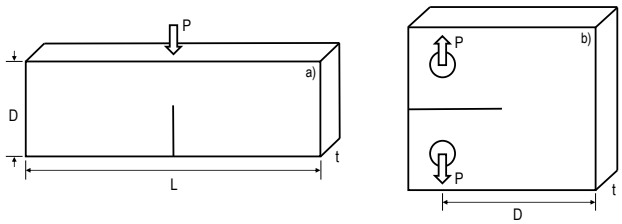

Figure 2. Schematic representation of the SENB and CT specimens considered in this work.

At incipient crack onset, the energy release rate ought to be equal to the fracture

energy of the material. Accordingly, the failure condition can now be written as:

$$G\left(\alpha_0 + c_f/D\right) = \frac{\sigma_{Nc}^2 D}{E^*} g\left(\alpha_0 + c_f/D\right) = G_f \tag{2}$$

where G_f is the mode I fracture energy of the material and c_f is the effective FPZ length, both assumed to be material properties. It should be remarked that this equation characterizes the peak load conditions if $g'(\alpha) > 0$, i.e. only if the structure has positive geometry [32].

By approximating $g\left(\alpha\right)$ with its Taylor series expansion at α_0 and retaining only up to the linear term of the expansion, one obtains:

$$G_f = \frac{\sigma_{Nc}^2 D}{E^*}\left[g(\alpha_0) + \frac{c_f}{D} g'(\alpha_0)\right] \tag{3}$$

which can be rearranged as follows [32]:

$$\sigma_{Nc} = \sqrt{\frac{E^* G_f}{D g(\alpha_0) + c_f g'(\alpha_0)}} \tag{4}$$

where $g'\left(\alpha_0\right) = \mathrm{d}g\left(\alpha_0\right)/\mathrm{d}\alpha$.

This equation, known as Bažant's Size Effect Law (SEL) [29, 30, 32, 33], relates the nominal strength to mode I fracture energy, a characteristic size of the structure, D, and to a characteristic length of the material, c_f, and it can be rewritten in the following form:

$$\sigma_{Nc} = \frac{\sigma_0}{\sqrt{1 + D/D_0}} \tag{5}$$

with $\sigma_0 = \sqrt{E^* G_f / c_f g'(\alpha_0)}$ and $D_0 = c_f g'(\alpha_0)/g(\alpha_0) =$ constant, depending on both FPZ size and specimen geometry. Contrary to classical LEFM, Eq. (5) is endowed with a characteristic length scale D_0. This is key to describe the transition from ductile to brittle behavior with increasing structure size.

Calculation of $g\left(\alpha\right)$ and $g'\left(\alpha\right)$

SINGLE EDGE NOTCH BENDING (SENB) SPECIMENS

The calculation of $g(\alpha)$ and $g'(\alpha)$ for SENB specimens can be done according to the procedure described in [12]. This leads to the following polynomial expressions:

$$g(\alpha) = 1155.4\alpha^5 - 1896.7\alpha^4 + 1238.2\alpha^3 - 383.04\alpha^2 + 58.55\alpha - 3.0796 \tag{6}$$

$$g'(\alpha) = 18909\alpha^5 - 31733\alpha^4 + 20788\alpha^3 - 6461.5\alpha^2 + 955.06\alpha - 50.88 \tag{7}$$

COMPACT TENSION (CT) SPECIMENS

In the case of CT specimens, the values for $g(\alpha)$ and $g'(\alpha)$ can be determined leveraging on the equations provided by ASTM D5045-99 [41]. Following the standard, the mode I Stress Intensity Factor (SIF), K_I, can be written as:

$$K_I = \frac{P}{t\sqrt{D}} f(\alpha) \tag{8}$$

where $\alpha = a/D$ and D is the distance between the center of hole to the end of the specimen as defined in ASTM D5045-99 [41] (see Fig. 2b). The nominal stress σ_N for CT specimens can be defined as:

$$\sigma_N = \frac{P}{tD} \tag{9}$$

The mode I Stress Intensity Factor can be rewritten as follows by combining Eq. (8) and Eq. (9):

$$K_I = \sqrt{D}\sigma_N f(\alpha) \tag{10}$$

By considering the relationship between energy release rate and stress intensity factor for a plane strain condition, the mode I energy release rate results into the following expression:

$$G_I = \frac{D\sigma_N^2}{E} g(\alpha) \tag{11}$$

where $g(\alpha) = f^2(\alpha)(1 - \upsilon^2)$, and $f(\alpha)$ is a dimensionless function accounting for geometrical effects and the finiteness of the structure (see e.g. [41]). Once $g(\alpha)$ is derived, the expression of $g'(\alpha)$ can be obtained by differentiation leading to the following polynomial expressions for $g(\alpha)$ and $g'(\alpha)$ respectively:

$$g(\alpha) = 33325\alpha^5 - 52330\alpha^4 + 32016\alpha^3 - 9019.1\alpha^2 + 1230.1\alpha - 51.944 \tag{12}$$

$$g'(\alpha) = 555868\alpha^5 - 895197\alpha^4 + 554047\alpha^3 - 159153\alpha^2 + 21035\alpha - 917.3 \tag{13}$$

FRACTURE BEHAVIOR OF THERMOSET NANOCOMPOSITES: ANALYSIS AND DISCUSSION

Fracture Scaling of Nanocomposites

To investigate the effects of the non-linear FPZ, the fracture tests on the thermoset polymer reinforced by nanoparticles in the literature are analyzed and discussed. Figure 3 shows the normalized structural strength σ_{Nc}/σ_0 in the literature and the fitting by SEL plotted as a function of the normalized structure size D/D_0 in double logarithmic scale. In such a graph, the structural scaling predicted by LEFM is represented by a line of slope $-1/2$ whereas the case of no scaling, as predicted by stress-based failure criteria, is represented by a horizontal line. The intersection between the LEFM asymptote, typical of brittle behavior, and the plastic asymptote, typical of ductile behavior, corresponds to $D = D_0$, called the *transitional size* [32].

As can be noted from Figure 3, the experimental data on nanocomposites almost distribute on the curve predicted by SEL. This shows that, for nanocomposites which lie close to the LEFM asymptote, the FPZ size has a negligible effect and LEFM can be applied, as suggested by ASTM D5045-99 [41]. However, this is not the case for those in the transitional range, which are characterized by a significant deviation from LEFM. This phenomenon can be ascribed to the increased size of the FPZ compared to the structure size which makes the non-linear effects caused by micro-damage in front of the crack tip not negligible.

As the experimental data show, LEFM does not always provide an accurate method to extrapolate the structural strength of larger structures from lab tests on small-scale specimens, especially if the size of the specimens belonged to the transitional zone. In fact, the use of LEFM in such cases may lead to a significant underestimation of structural strength, thus hindering the full exploitation of graphene nanocomposite fracture properties. This is a severe limitation in several engineering applications such as e.g. aerospace or aeronautics for which structural performance optimization is of utmost importance. On the other hand, LEFM always overestimates significantly the strength when used to predict the structural performance at smaller length-scales. This is a serious issue for the design of e.g. graphene-based MEMS and small electronic components or nanomodified carbon fiber composites in which the inter-fiber distance occupied by the resin is only a few micrometers and it is comparable to the FPZ size. In such cases, SEL or other material models characterized by a characteristic length scale ought to be used.

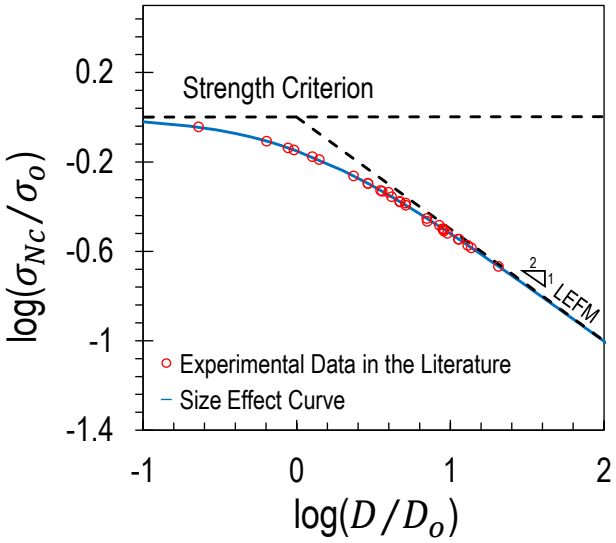

Figure 3. Size effect curves for nanocomposites measured from fracture tests in the literature.

Effects of a finite FPZ on the calculation of Mode I fracture energy

Notwithstanding the importance of understanding the scaling of the fracturing behavior, the tests conducted by Mefford *et al*. [12] represent, to the best of the authors' knowledge, the only comprehensive investigation on the size effect in nanocomposites available to date. All the fracture tests reported in the literature were conducted on one size and analyzed by means of LEFM. Considering the remarkable effects of the nonlinear FPZ on the fracturing behavior documented in the foregoing section, it is interesting to critically re-analyze the fracture tests available in the literature by means of SEL. This formulation is endowed with a characteristic length related to the FPZ size and, different from LEFM, it has been shown to accurately capture the transition from brittle to quasi-ductile behavior of nanocomposites.

APPLICATION OF SEL TO THERMOSET POLYMER NANOCOMPOSITES

To understand if the quasi-brittle behavior reported in previous tests [12] is a salient feature of graphene nanocomposites only or if it characterizes other nanocomposites, a large bulk of literature data were re-analyzed by SEL using Eq.(3) in order to study the effects of the FPZ. In this analysis, in the absence of data on the effective FPZ length, c_f, in the literature, it is assumed that $c_f = 0.44 l_{ch}$ which, according to Cusatis *et al.* [34], corresponds to the assumption of a linear cohesive law. In this expression, $l_{ch} = E^* G_f / f_t^2$ is Irwin's characteristic length which depends on Young's modulus E^*, the mode I fracture energy G_f and the ultimate strength of the material f_t. Substituting this expression into Eq. (3) and rearranging one gets the following expression which relates the fracture energy calculated according to SEL to the fracture energy calculated by LEFM:

$$G_{f,SEL} = \frac{G_{f,LEFM}}{1 - \frac{0.44 E^* g'(\alpha_0) G_{f,LEFM}}{D f_t^2 g(\alpha_0)}} \tag{14}$$

In this equation, $G_{f,LEFM} = \sigma_{Nc}^2 D g(\alpha_0) / E^*$ represents the fracture energy which can be estimated by analyzig the fracture tests by LEFM.

It can be observed from Eq.(14) that the correct fracture energy in the literature can be calculated by knowing three key parameters provided that $g(\alpha)$ and $g'(\alpha)$ are known: (1) the fracture energy through the use of LEFM; (2) the Young's modulus of the specimens at different nanoparticle concentrations; and (3) the ultimate strength of the specimens at different nanoparticle concentrations. For cases in which those parameters were not provided by the authors, the ultimate strength, Young's modulus, and Poisson's ratio of nanocomposites were reasonably assumed to be 50 MPa, 3000 MPa, and 0.35 respectively.

MODE I FRACTURE ENERGY OF THERMOSET POLYMER NANOCOMPOSITES

Several types of nanofillers were investigated in this re-analysis including carbon-based nano-fillers (such as carbon black, graphene oxide, graphene nanoplatelets, and multi-wall carbon nanotubes), rubber and silica nanoparticles, and nanoclay. The fracture energy estimated from LEFM compared to the calculation through SEL, Eq. (14), for nanomodified SENB and CT specimens are plotted in Figures 4-6 along with the highest difference.

Figure 4 shows data elaborated from Carolan *et al.* [13] who conducted fracture tests on SENB specimens nano-modified by six different combinations of nanofillers. As can be noted, while for the pristine polymer the difference between LEFM and SEL is negligible, this is not the case for the nanomodified polymers, the difference increasing with increasing nanofiller content. The difference varies based on the type of nanofiller used, with the greatest value being 42.6% for the addition of 8 wt% core shell rubber mixed with 25% diluent and 8% silica. This remarkable number confirms that for the SENB specimens tested in [13] the nonlinear behavior of the FPZ was not negligible, leading to a more ductile behavior compared to the pristine polymer.

Similar conclusions can be drawn based on Figures 5a-f which report the analysis of fracture tests conducted by Zamanian *et al.* [14] and Jiang *et al.* [8] on polymers reinforced by silica nanoparticles and silica nanoparticle+graphene oxide respectively. For the data in [14], the greatest percent difference of fracture energy between LEFM and SEL decreased as the size of silica nanoparticle increased, with the greatest difference being 28% for the addition of 6 wt% 12 nm silica nanoparticles. For all the systems investigated, the maximum deviation from LEFM was for the largest amount of nanofiller, confirming that nanomodification lead to larger FPZ sizes and more pronounced ductility. On the other hand, the data by Jiang *et al.* [8] exhibit an even larger effect of the FPZ with the greatest difference in fracture energy between LEFM and SEL reaching up to 51.8% for silica nanoparticle attached to graphene oxide.

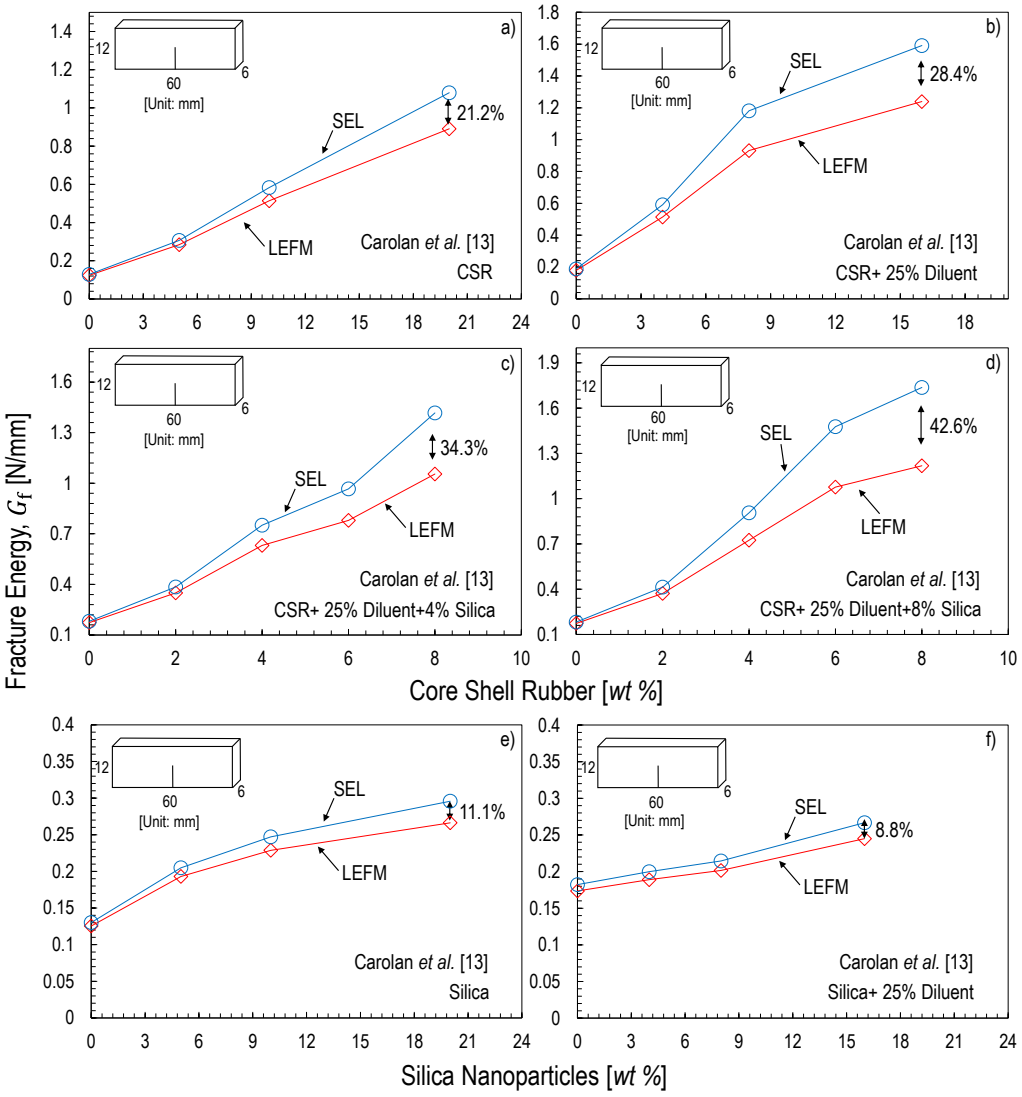

Figure 4. Mode I fracture energy estimated by Linear Elastic Fracture Mechanics (LEFM) and Size Effect Law (SEL), Eq. (14). The latter formulation accounts for the finite size of the nonlinear Fracture Process Zone (FPZ) in thermoset nanocomposites. Data re-analyzed from [13].

Figure 6 shows a re-analysis of the data reported by Liu *et al.* [19] who tested CT specimens nano-modified by four different combinations of silica nanoparticle and rubber. As can be noted, in this case, the FPZ indeed affects the fracturing behavior significantly. Adopting LEFM, which assumes the size of the FPZ to be negligible, for the estimation of G_f from the fracture tests would lead to an underestimation of up to 156.8% for the case of polymer reinforced by 15 wt% rubber only. This tremendous difference, the largest found in the present study, gives a tangible idea on the importance of accounting for the nonlinear damage phenomena occurring in nanocomposites which can lead to a significant deviation from the typical brittle behavior of thermoset polymers.

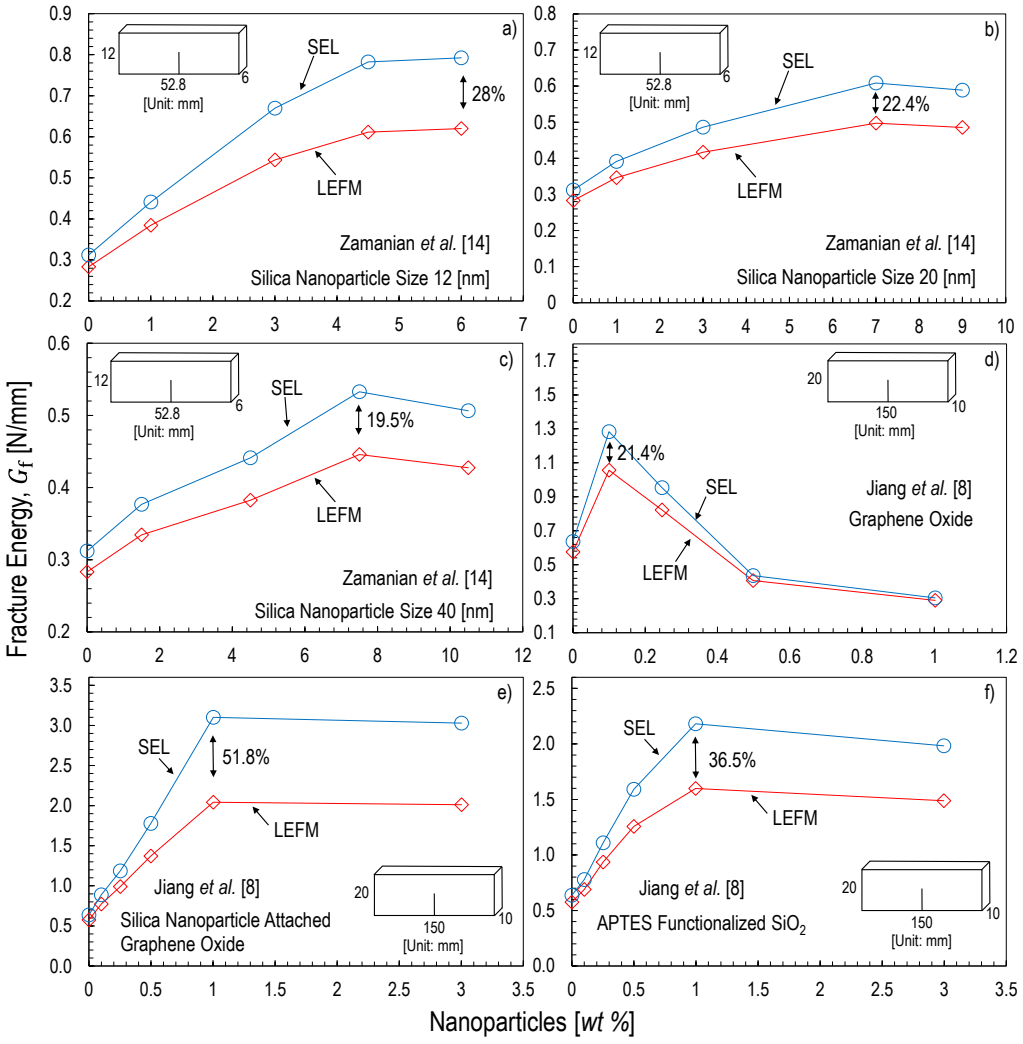

Figure 5. Mode I fracture energy estimated by Linear Elastic Fracture Mechanics (LEFM) and Size Effect Law (SEL), Eq. (14). The latter formulation accounts for the finite size of the nonlinear Fracture Process Zone (FPZ) in thermoset nanocomposites. Data re-analyzed from [14] and [8].

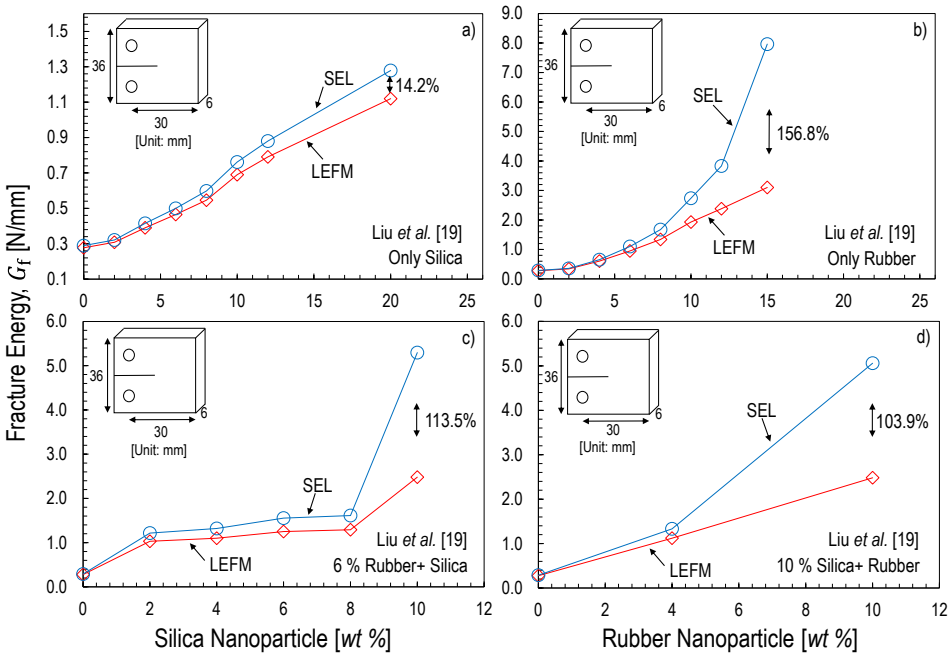

Figure 6. Mode I fracture energy estimated by Linear Elastic Fracture Mechanics (LEFM) and Size Effect Law (SEL), Eq. (14). The latter formulation accounts for the finite size of the nonlinear Fracture Process Zone (FPZ) in thermoset nanocomposites. Data re-analyzed from [19].

COHESIVE ZONE MODELING ON THERMOSET NANOCOMPOSITES

To have a further understanding on the fracture behavior of nanocomposites, a cohesive crack modeling was used in ABAQUS Explicit 2017. To this end, as illustrated in Figure 7, a Single Edge Notch Bending (SENB) specimen was simulated by using 4-node two dimensional cohesive elements (COH2D4) with a traction-separation model in the middle and 4-node bilinear plain strain quadrilateral elements (CPE4R) with a linear elastic isotropic constitutive model at two sides, which subjects to the displacement on the middle top of the specimen. It is worth mentioning here that the width of crack was modeled as 4 μm based on the image obtained from Scanning Electron Microscopy (SEM).

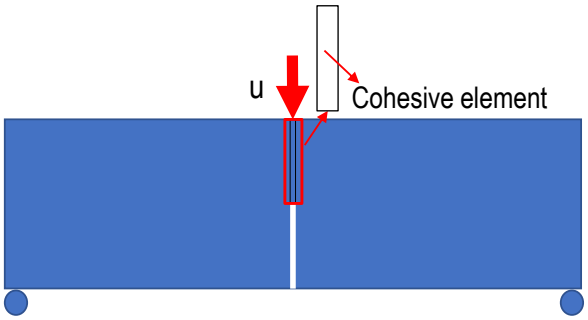

Figure 7. Schematic cohesive crack modeling.

Linear Cohesive Crack Law

The following fracture energies were used in a linear cohesive crack modeling to further verify the forgoing method (Eq.(14)) discussed in the previous section: (1) G_f calculated by LEFM; (2) G_f corrected by Eq.(14). As can be noted from Figure 8, a linear cohesive crack modeling using corrected G_f is capable of capturing the experimental data in the literature. However, this is not the case if G_f by LEFM is used in a linear cohesive modeling, with the non-negligible underestimation on the peak load of investigated nanocomposites. This is the confirmation that Size Effect Law (SEL) can be adapted to re-analyze the fracture tests available in the literature.

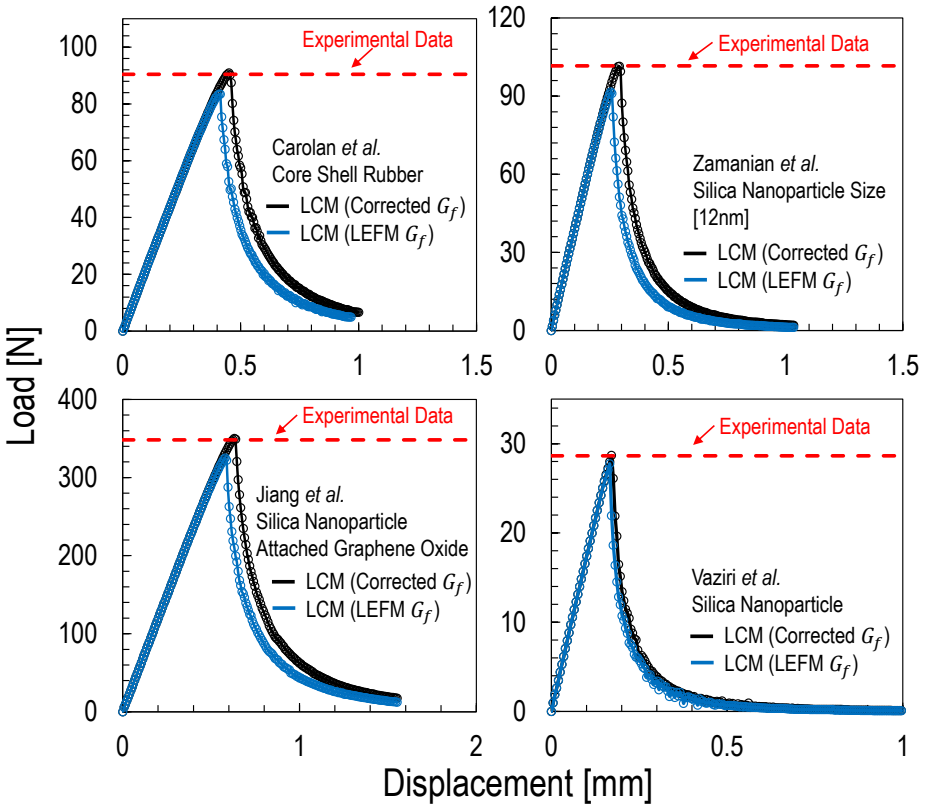

Figure 8. Load-displacement curves obtained by using a linear cohesive crack law with both LEFM and corrected G_f on the re-analysis of data from [8], [13, 14] and [17].

By leveraging on a linear cohesive crack modeling with the corrected G_f, the fracturing behavior on the scaling of nanocomposites can be predicted without additional tests in the lab. As Figure 9 shows, for large specimen sizes, the prediction on the peak load of investigated nanocomposites by using LEFM G_f leads to a significant underestimation. It is worth mentioning here that this analysis is on the assumption that nanocomposites in the literature follow a linear cohesive crack law. However, it was shown that the invesigated graphene nanocomposite was characterized by a bilinear cohesive law. In this case, the underestimation on the peak load of nanocomposites using G_f calculated by LEFM is remarkable.

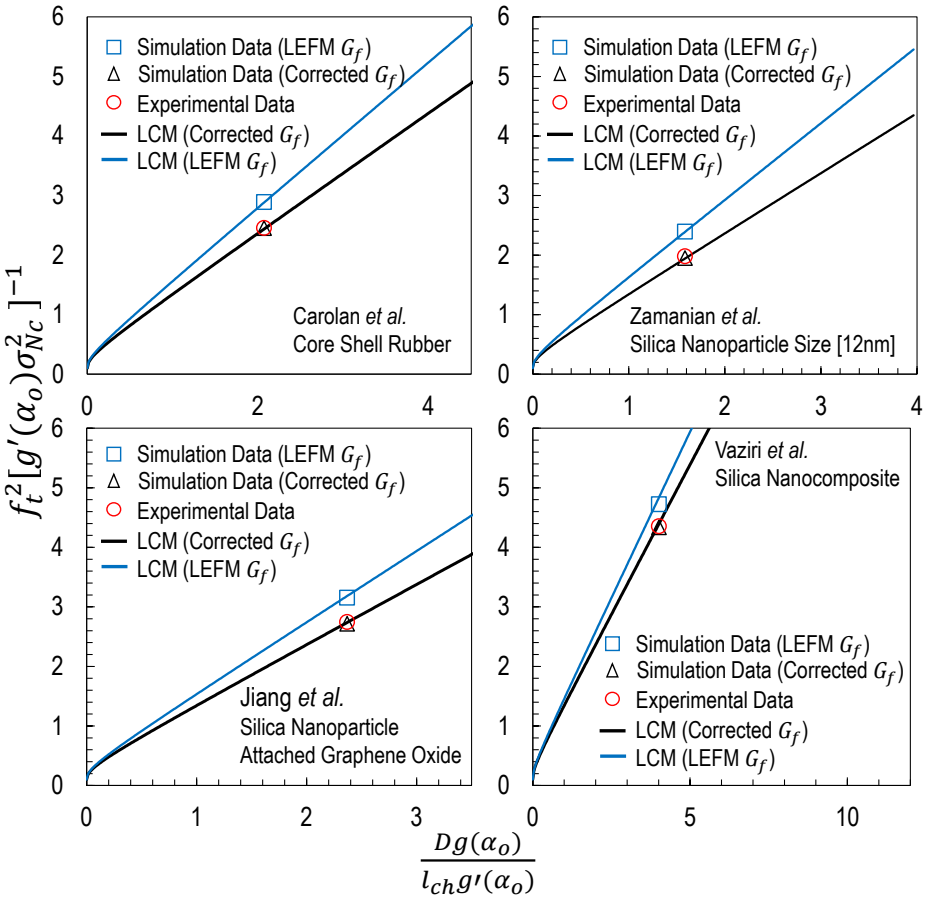

Figure 9. Comparison between experimental data and LCM results on the re-analysis of data from [8], [13, 14] and [17].

Bilinear Cohesive Crack Law

Thanks to the comprehensive investigation on the size effect in graphene nanocomposites by Mefford *et al* [12], the importance on the determination of a unique cohesive crack law can be further studied. To this end, both linear and bilinear cohesive laws with the same fracture energy were used to match load-displacement curves obtained from experimental fracture tests on geometrically scaled Single Edge Notch Bending (SENB) specimens with varying contents of graphene. It is worth mentioning here that, for bilinear cohesive law with the same fracture energy, different intersection points where the slope of cohesive stress changes are investigated in order to match experimental load-displacement curves.

It was shown, as illustrated in Figures 10-11, while the bilinear cohesive crack law successfully matches experimental curves of specimens with different sizes and graphene concentrations, this is not the case for linear cohesive crack law, with a significant overestimation from experimental curves. This may indicates that some of investigated nanocomposites available in the literature follow a bilinear cohesive crack law. Thus, to have an accurate re-analysis on the fracture tests in a large bulk of literature without additional tests in the lab, bilinear cohesive crack law needs to be further studied.

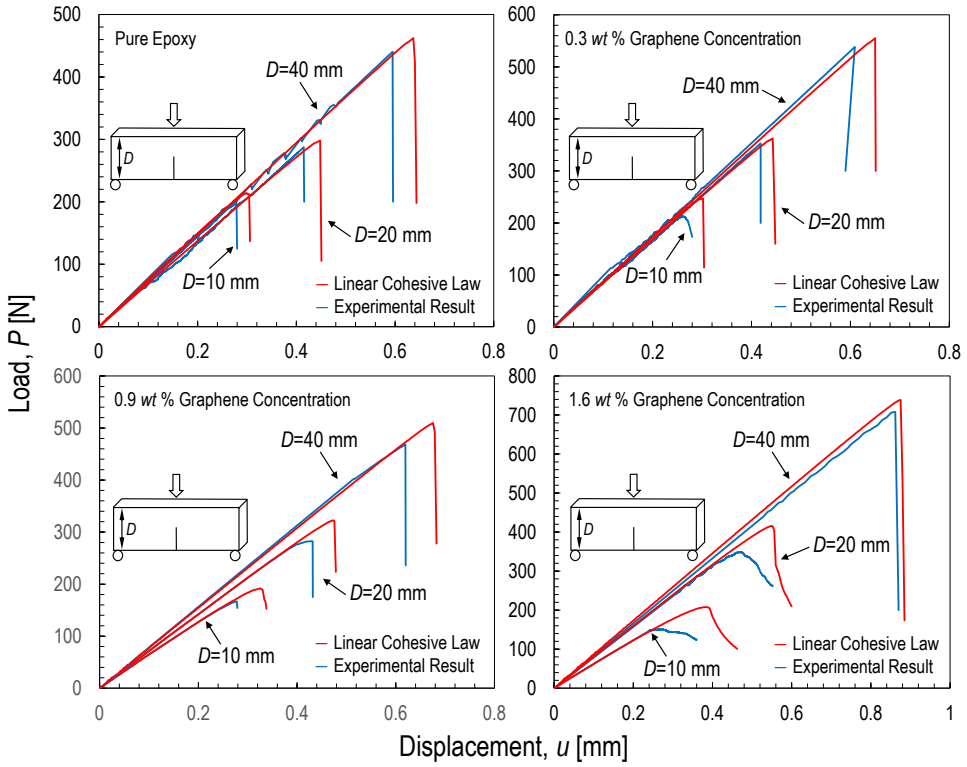

Figure 10. Load-displacement curves vs. linear cohesive simulation for different graphene contents and specimen sizes.

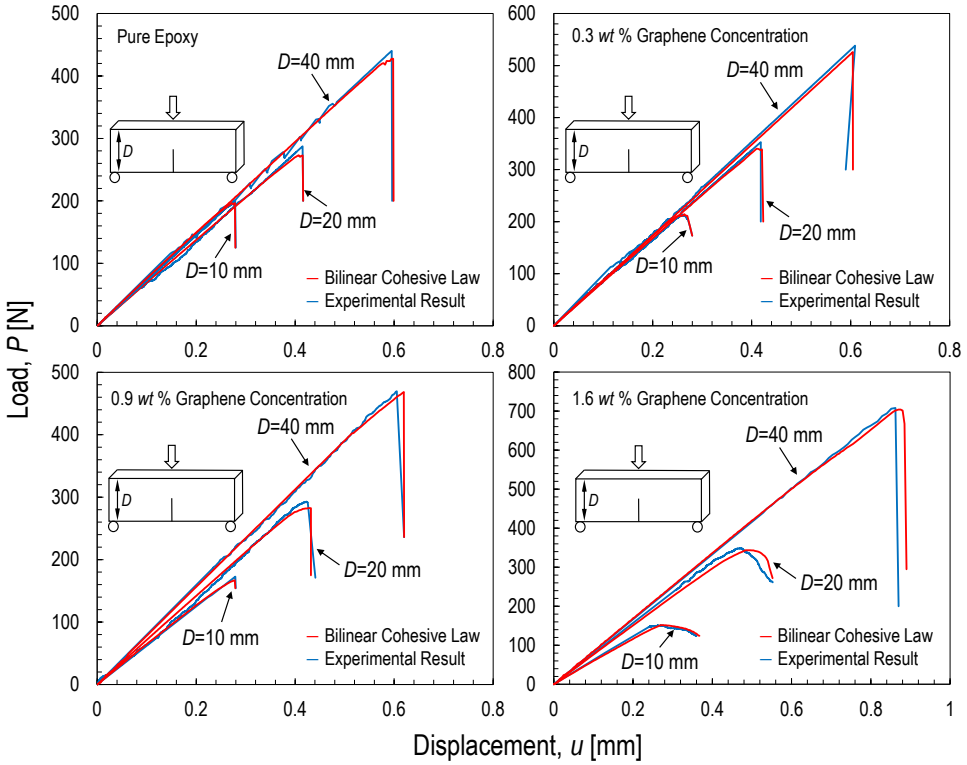

Figure 11. Load-displacement curves vs. bilinear cohesive simulation for different graphene contents and specimen sizes.

Through the bilinear cohesive crack analysis, as illustrated in Figure 12, it is interesting to note that the initial fracture energy of calibrated bilinear cohesive law does not increase significantly as a function of graphene content, which implies the fact that the improvement of mechanical behavior of small-scale nanocomposite structure depends on the strength other than fracture energy whereas improvement of large-scale structure depends on fracture energy.

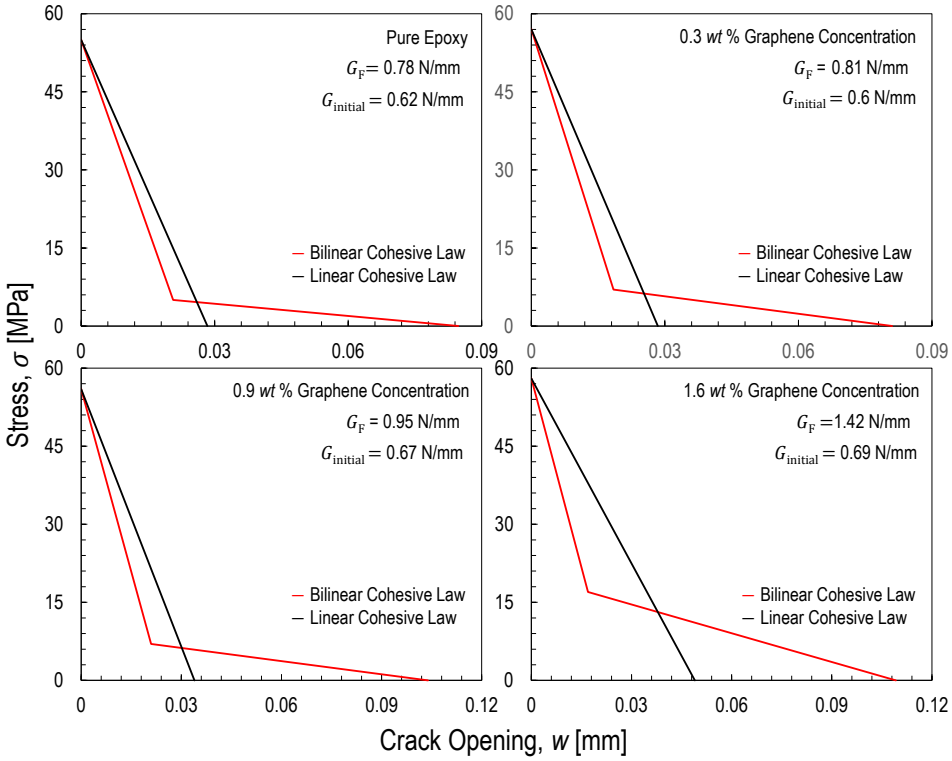

Figure 12. Calibrated bilinear cohesive law vs. linear cohesive law with the same fracture energy..

CONCLUSION

Leveraging a large bulk of literature data, this paper investigated the effects of the Fracture Process Zone (FPZ) on the fracturing behavior of thermoset polymer nanocomposites, an aspect of utmost importance for structural design but so far overlooked. Based on the results obtained in this study, the following conclusions can be elaborated:

1. The double logarithmic plots of the normalized structural strength as a function of the normalized characteristic size of geometrically-scaled SENB specimens showed that the experimental data on nanocomposites available in the literature distribute on the curve predicted by SEL. Most of nanocomposites are located in the transitional range in which the fracturing behavior can not be characterized by Linear Elastic Fracture Mechanics (LEFM);

2. By employing Size Effect Law and assuming a linear cohesive behavior [34], a large bulk of literature data on the mode I fracture energy of thermoset nanocom-

posites was critically re-analyzed. It was shown that for most of the fracture tests in the literature, the effects of the nonlinear FPZ are not negligible, leading to significant deviations from LEFM. As the data indicate, this aspect needs to be taken into serious consideration since the use of LEFM to estimate mode I fracture energy can lead to an error as high as 156% depending on the specimen size and nanofiller content;

3. The deviation from LEFM reported in the re-analyzed results is related to the size of the Fracture Process Zone (FPZ) for increasing contents of nanofiller. In the pristine polymer the damage/fracture zone close to the crack tip, characterized by significant non-linearity due to subcritical damaging, was generally very small compared to the specimen sizes investigated. This was in agreement with the inherent assumption of LEFM of negligible non-linear effects during the fracturing process. However, the addition of nano-fillers results in larger and larger FPZs. For sufficiently small specimens, the size of the highly non-linear FPZ was not negligible compared to the specimen characteristic size thus highly affecting the fracturing behavior, this resulting into a significant deviation from LEFM;

4. A linear cohesive crack modeling was conducted to re-analyze the fracture tests available in the literature. It was shown that the experimental data was successfully captured by a LCM with the fracture energy corrected by Eq.(14) considering the non-negligible effects of FPZ. However, this is not the case for a LCM with the frature energy calculated by LEFM assuming the FPZ to be a materematical point. More importantly, the prediction on the peak load of nanocomposites by using a linear cohesive law with the fracture energy calculated by LEFM leads to a significant underestimation;

5. Thanks to the fracture tests on the scaling of graphene nanocomposites reported by Mefford *et al* [12], it was found that graphene nanocomposite specimens with different sizes and concentrations follow a bilinear cohesive crack law.

REFERENCES

1. Rogers JA. Electronic materials: making graphene for microelectronics. Nat Nanotechnol 2008;3(5):254-55.

2. Yoo EJ, Kim J, Hosono E, Zhou HS, Kudo T, Honma I. Large Reversible Li Storage of Graphene Nanosheet Families for Use in Rechargeable Lithium Ion Batteries. Nano Lett 2008;8:2277-82

3. Chien CT, Hiralal P, Wang DY, Huang IS, Chen CC, Chen CW, Amaratunga GA.J. Graphene-Based Integrated Photovoltaic Energy Harvesting/Storage Device. Small 2015;11:2929-37.

4. Zhang JF, Ryu S, Pugno N, Wang QM, Tu Qing, Buehler MJ, Zhao XH. Multifunctionality and control of the crumpling and unfolding of large-area graphene. Nat Mater 2013;12:321.

5. Kuila T, Bose S, Khanra P, Mishra AK, Kim NH, Lee JH. Recent advances in graphene-based biosensors. Biosens Bioelectron 2011;26:4637-48.

6. Balandin AA, Ghosh S, Bao WZ, Calizo I, Teweldebrhan D, Miao F, Lau CN. Superior thermal conductivity of single-layer graphene. Nano Lett 2008;8:902-7.

7. Ramirez C, Figueiredo FM, Miranzo p, Poza p, Osendi MI. Graphene nanoplatelet/silicon nitride composites with high electrical conductivity. Carbon 2012;50:3607-15.

8. Jiang T, Kuila T, Kim NH, Ku BC, Lee JH. Enhanced mechanical properties of silanized silica nanoparticle attached graphene oxide/epoxy composites. Compos Sci Technol 2013;79:115-25.

9. Konnola R, Nair CPR, Joseph K. High strength toughened epoxy nanocomposite based on poly(ether sulfone)-grafted multi-walled carbon nanotube. Polym Advan Technol 2015;27:82-89.

10. Zappalorto M, Salviato M, Quaresimin M. Mixed mode (I+II) fracture toughness of polymer nanoclay nanocomposites. Eng Fract Mech 2013;111:50-64.

11. Zappalorto M, Salviato M, Pontefisso A, Quaresimin M. Notch effect in clay-modified epoxy: a new perspective on nanocomposite properties. Compos Interfaces 2013;20:405-19.

12. Mefford C, Qiao Y, Salviato M. Failure behavior and scaling of graphene nanocomposites, Compos Struct 2017;176:961-72.

13. Carolan D, Ivankovic A, Kinloch AJ, Sprenger S, Taylor AC. Toughening of epoxy-based hybrid nanocomposites. Polymer 2016;97:179-190.

14. Zamanian M, Mortezaei M, Salehnia B, Jam JE. Fracture toughness of epoxy polymer modified with nanosilica particles: particle size effect. Eng Fract Mech 2013;97:193-206.

15. Chandrasekaran S, Sato N, Tölle F, Mülhaupt R, Fiedler B, Schulte K. Fracture toughness and failure mechanism of graphene based epoxy composites. Compos Sci Technol 2014;97:90-99.

16. Kim BC, Park SW, Lee DG. Fracture toughness of the nano-particle reinforced epoxy composite. Compos Struct 2008;86:69-77.

17. Vaziri HS, Abadyan M, Nouri M, Omaraei IA, Sadredini Z, Ebrahimnia M. Investigation of the fracture mechanism and mechanical properties of polystyrene/silica nanocomposite in various silica contents. J Mater Sci 2011;46:5628-38.

18. Dittanet P, Pearson R. Effect of silica nanoparticle size on toughening mechanisms of filled epoxy Polymer 2012;53:1890-1905.

19. Liu HY, Wang GT, Mai YW, Zeng Y. On fracture toughness of nano-particle modified epoxy. Compos Part B-Eng 2011;42:2170-75.

20. Zhang H, Tang LC, Zhang Z, Friedrich K, Sprenger S. Fracture behaviors of in situ silica nanoparticle-filled epoxy at different temperatures. Polymer 2008;49:3816-25.

21. Johnsen BB, Kinloch AJ, Mohammed RD, Taylor AC, Sprenger S. Toughening mechanisms of nanoparticle-modified epoxy polymers. Polymer 2007;48:530-41.

22. Wang X, Jin J, Song M. An investigation of the mechanism of graphene toughening epoxy. Carbon 2013;65:324-33.

23. Chandrasekaran S, Seidel C, Schulte K. Preparation and characterization of graphite nano-platelet (GNP)/epoxy nano-composite: mechanical, electrical and thermal properties. Eur Polym J 2013;49:3878-88.

24. Naous W, Yu XY, Zhang QX, Naito K, Kagawa y. Morphology, tensile properties and fracture toughness of epoxy/Al_2O_3 nanocomposites. J Polym Sci Pol Phys 2006;44:1466-73.

25. Wetzel B, Rosso P, Haupert F, Friedrich K. Epoxy nanocomposites-fracture and toughening mechanisms. Eng Fract Mech 2006;73:2375-98.

26. Quaresimin M, Salviato M, Zappalorto M. Toughening mechanisms in nanoparticle polymer composites: experimental evidences and modeling." In book: Toughening Mechanisms in Composite Materials 2015; 113-33.

27. Quaresimin M, Salviato M, Zappalorto M. Fracture and interlaminar properties of clay-modified epoxies and their glass reinforced laminates. J Eng Mech 2012; 81: 80-93.

28. Pathak AK, Borah M, Gupta A, Yokozeki T, Dhakate SR, Improved mechanical properties of carbon fiber/graphene oxide-epoxy hybrid composites. Compos Sci Technol 2016;135:28-38.

29. Bažant ZP. Size effect in blunt fracture: concrete, rock, metal. J Eng Mech-ASCE 1984;110:518-35.

30. Bažant ZP, Kazemi MT. Determination of fracture energy, process zone length and brittleness number from size effect, with application to rock and concrete. Int J Fracture 1990;44:111-31.

31. Bažant ZP, Daniel IM, Li Z. Size effect and fracture characteristics of composite laminates. J Eng Mater-T ASME 1996;118:317-24.

32. Bažant ZP, Planas J. Fracture and size effect in concrete and other quasi-brittle materials. Boca Raton:CRC Press;1998.

33. Salviato M, Kirane K, Ashari SE, Bažant ZP. Experimental and numerical investigation of intra-laminar energy dissipation and size effect in two-dimensional textile composites. Compos Sci Technol 2016;135:67-75.

34. Cusatis G, Schauffert EA, Cohesive crack analysis of size effect, Eng Fract Mech 2009; 76:2163-73.

35. Salviato M, Zappalorto M, Quaresimin M. Plastic yielding around nanovoids, Procedia Engineer 2011;10:3316-21.

36. Chandrasekaran S, Sato N, Tlle F, Mlhaupt R, Fiedler B, Schulte K. Fracture toughness and failure mechanism of graphene based epoxy composites. Compos Sci Technol 2014;97:909.

37. Salviato M, Zappalorto M, Quaresimin M. Plastic shear bands and fracture toughness improvements of nanoparticle filled polymers: a multiscale analytical model. Compos Part A - Appl S 2013;48:144-52.

38. Salviato M, Zappalorto M, Quaresimin M. Nanoparticle debonding strength: a comprehensive study on interfacial effects. Int J Solids Struct 2013;50:3225-32.

39. Quaresimin M, Salviato M, Zappalorto M. A multi-scale and multi-mechanism approach for the fracture toughness assessment of polymer nanocomposites. Compos Sci Technol 2014;91:16-21.

40. Quaresimin M., Schulte K., Zappalorto M., Chandrasekaran S., Toughening mechanisms in polymer nanocomposites: From experiments to modelling, Compos Sci Tech 2016;123:187-204.

41. ASTM D5045-99 - Standard Test Methods for Plane-Strain Fracture Toughness and Stain Energy Release Rate of Plastic Materials 1999.